Available online at www.sciencedirect.com
SCIENCE DIRECT
Journal of the European Ceramic Society 26 (2006) 1141–1148
www.elsevier.com/locate/jeurceramsoc

Crystal phase separation and microstructure of a thermally treated vitrified solid waste

Th. Kehagias [a,*], Ph. Komninou [a], P. Kavouras [a], K. Chrissafis [a], G. Nouet [b], Th. Karakostas [a]

[a] *Physics Department, Aristotle University of Thessaloniki, 541 24 Thessaloniki, Greece*
[b] *ENSICAEN/SIFCOM UMR CNRS 6176, 6 Boulevard du Maréchal Juin, 14050 Caen, Cedex, France*

Received 4 November 2004; received in revised form 27 December 2004; accepted 16 January 2005
Available online 21 February 2005

Abstract

The vitrification method was used to stabilize a solid industrial waste residue rich in iron and lead oxides. Upon devitrification of the glass products, the effect of batch composition on the ability to produce glass-ceramic materials was investigated by electron microscopy techniques. The crystallization and microstructural evolution of the vitreous products was explored with respect to the annealing conditions. In the course of vitrification, ferric oxide functioned as a glass network former, contributing to the structural integrity of the vitreous matrix. After thermal treatment of the vitrified products, at temperatures determined by differential thermal analysis, $Pb_8Fe_2O_{11}$, $PbFe_{12}O_{19}$ and Fe_2O_3 were the dominant crystal phases detected in the glass-ceramic products, the former characterized as a new structure. The distribution of iron and lead oxides among different crystalline phases was found to be the dominant parameter determining the efficiency of lead captivation into the volume of the devitrified products, whereas in glass products lead is diffused in the amorphous matrix.

Keywords: Electron microscopy; Microstructure-final; Glass-ceramics; Waste materials

1. Introduction

Vitrification of hazardous industrial wastes exploiting low-cost vitrifying agents, for the production of vitreous and glass-ceramic materials, has drawn considerable scientific and technological attention. The vitrification method has been accepted as one of the most appropriate techniques for the stabilization of various wasteforms and solid residues from waste incineration,[1] since the rising environmental and economic costs of land filling disposal are considered prohibitively high. Vitrification concentrates a number of important merits such as, large waste volume reduction, low-cost application, negligible mass of by-products and the ability to produce marketable materials. It is also a well-tested method that has been successfully applied for the stabilization of urban, municipal, industrial, natural and radioactive waste forms.[2–9]

Vitrification products can be either vitreous or glass-ceramic, depending on the batch composition, temperature and duration of co-melting. Devitrification is an important part of the stabilization process, only if can be controlled to produce glass-ceramic materials with superior mechanical properties. It occurs spontaneously in the canister after melt casting or deliberately during thermal annealing. In the latter case, it is necessary that the devitrification process must not impair the chemical resistance achieved via vitrification. Post-annealing chemical stability depends on the distribution of the toxic element or compound in the microstructure of the glass-ceramic product. It has been shown that leach resistance is increased in the following cases: (a) when the polluting agent is entrapped in glassy islands shielded from a crystalline matrix[10] and (b) when it participates in the formation of crystal phases that have grown in a stable vitreous matrix.[11]

We have recently presented the course of stabilization of a hazardous solid waste rich in lead and iron oxides, which originates from petrochemical distillery facilities.[11–13] The mate-

* Corresponding author. Tel.: +30 2310 99 80 23; fax: +30 2310 99 85 89.
E-mail address: kehagias@auth.gr (Th. Kehagias).

0955-2219/$ – see front matter © 2005 Elsevier Ltd. All rights reserved.
doi:10.1016/j.jeurceramsoc.2005.01.047

rial subjected to vitrification consisted of solid residues from the incineration of sludge, recovered from storage tanks of tetraethyl lead (TEL) and leaded gasoline, with silica (SiO_2) and soda (Na_2CO_3) powders. Vitrification of the ash gave rise to the production of chemically stabilized vitreous materials, according to the United States Environmental Protection Agency (USEPA) standards, as it was found by applying the Toxicity Characteristic Leaching Procedure (TCLP) testing.[11] The as-quenched products have undergone a series of different annealing processes, in order to estimate their susceptibility to devitrification. The as-casted and devitrified products have been morphologically and structurally characterized in the macroscopic and mesoscopic levels,[11,12] while the evaluation of their mechanical properties[13] has proved they can be used for construction applications. However, in order to establish a correlation between the macroscopic physical properties and the microstructure of the as-quenched and devitrified products, a thorough investigation of the structure, in the microscopic and atomic levels, needs to be undertaken.

The aim of the present work was to examine the evolution of crystallization during thermal treatment of the fully vitrified waste residues and the microstructure of the devitrified products with electron microscopy (EM) techniques. Furthermore, we investigated the conditions under which iron oxide takes part in the construction of the glass network, and the way that lead is stabilized in the devitrified products. The devitrification process was thoroughly investigated by scanning, transmission and high-resolution transmission electron microscopy (SEM, TEM and HRTEM, respectively). EM techniques can provide, directly, valuable information on the microstructure, morphology and elemental composition in the microscopic and sub-microscopic levels. Additionally, materials' features obtained from EM can be connected to their engineering properties in a more straightforward manner, e.g. the mechanical properties with the morphological characteristics in the microscopic level. As a result, the use of EM techniques sufficiently supports the understanding of the issues under investigation.

2. Experimental procedure

The homogeneity of the vitrified products was inspected by optical microscopy and SEM. SEM observations were conducted in a JEOL JSM-840A microscope, equipped with an Oxford ISIS-300 energy dispersive spectrometry (EDS) analyzer. The temperatures of the annealing processes were determined by differential thermal analysis (DTA) of the vitrified products. DTA scans were obtained with a Setaram TG-DTA SetSys 1750 °C instrument in Argon atmosphere. Heating and cooling rates were set at 10 °C/min. The devitrification process, unless otherwise stated, comprised a heating stage with a temperature gradient of 10 °C/min, an isothermic stage of half an hour and a rapid cooling stage that was performed by removing the samples from the furnace. Specimens for TEM and HRTEM investigations were initially thinned by the standard procedure of mechanical grinding. Perforation of the specimens was achieved by chemical thinning in an appropriate bath consisted of 5% HF, 10% HCl and 85% H_2O. This method was employed for the structural characterization of the separated crystal phases, since HF and HCl preferentially attack the vitreous matrix.[14] TEM and HRTEM observations were carried out in a JEOL JEM-100CX and a JEOL JEM-2010 electron microscopes, operated at 100 and 200 kV, respectively, the latter equipped with a Link EDS microprobe analyzer capable of analyzing particles of a few nanometers size. The microprobe analysis was employed complementary to the EDS analysis by SEM, where higher local resolution was demanded.

3. Results

3.1. The microstructure of the vitreous products

Batch compositions prepared to study ash stabilization into a vitreous matrix are depicted in Table 1. Vitrification of the *W40*, *W50* and *W60* batch compositions resulted in vitreous products. A characteristic TEM micrograph of the as-poured *W40* product is illustrated in Fig. 1. The diffuse halo around the transmitted spot of the electron diffraction pattern, given as inset, as well as the lack of detectable contrast in the matrix, suggests the production of an amorphous material. Furthermore, HRTEM observations did not show any structural elements in the glassy matrices. The degree of homogeneity in the glass products was confirmed by SEM EDS analyses, where the composition variation of the constituent elements was comparable to the accuracy of the method, namely ±1 at.%. In addition, EDS microprobe analyses have proved that the lead content of the incinerated waste is dispersed throughout the vitreous matrix. The structural characteristics of all as-quenched products, inspected by EM techniques and the corresponding Si/O ratios are given in Table 1.

The specific vitrification process of the *W70* batch composition resulted in the production of a multiphase material,

Table 1
Results of the vitrification process on all batch compositions

Vitrified product	Ash (wt.%)	SiO_2 (wt.%)	Na_2O (wt.%)	Si/O ratio	Separated crystal phases	Structure
W40	40	50	10	0.37	–	Vitreous-homogeneous
W50	50	35	15	0.30	–	Vitreous-homogeneous
W60	60	25	15	0.25	–	Vitreous-inhomogeneous
W70	70	20	10	0.22	Hematite + magnetite	Multiphase-inhomogeneous

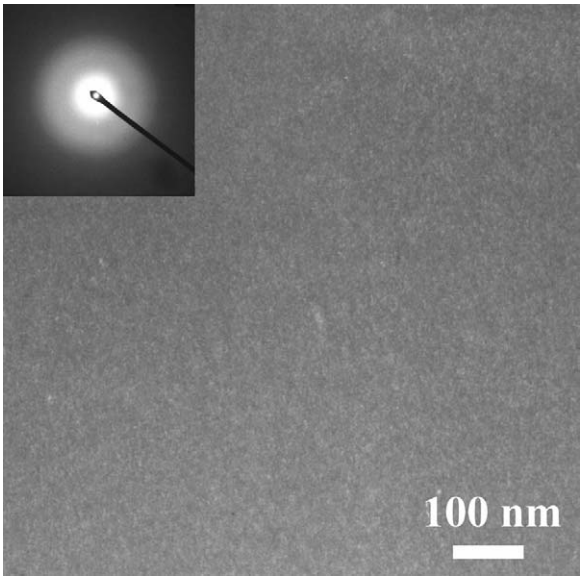

Fig. 1. Bright field (BF) TEM micrograph of the *W40* glass, showing a homogeneous contrast of the vitreous matrix. The corresponding diffraction pattern is characteristic of an amorphous material.

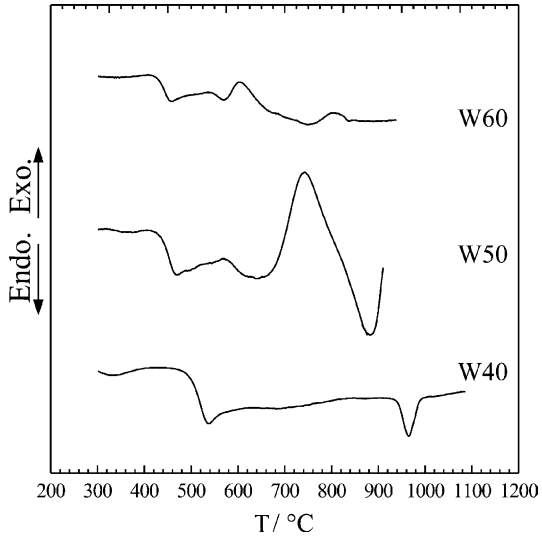

Fig. 3. DTA thermographs of the amorphous as-vitrified products illustrating the different phase changes of the material.

where iron oxide was separated from the amorphous matrix in the form of ferric and ferrous oxides as needle-like crystallites.[11] The elemental composition of the matrix was highly depended on the proximity to the crystallites. The EDS analysis showed that regions near crystallites contained 40% less iron compared with remote matrix areas. A thin slice of *W70* observed by optical microscopy under transmitted illumination is presented in Fig. 2(a). Opaque polycrystalline regions, denoted by I, correspond to rich in iron areas, in respect to transparent glassy regions, denoted by II. TEM observations revealed that opaque regions are polycrystalline areas, where crystallites of hematite and magnetite have been separated. This is shown in Fig. 2(b), where a bright field (BF) TEM image of an opaque region characteristic of a polycrystalline structure is presented. The degree of crystallinity was estimated at ≅60% by measuring the total area corresponding to needle-like crystals and crystallites from ten mechanically polished sections utilizing optical microscopy. Since *W70* was not fully vitrified, due to the high content of waste, it was not further investigated in this work.

3.2. Determination of thermal treatment temperatures

In order to devitrify all as-quenched vitreous products, DTA thermographs were obtained for *W40, W50* and *W60* glass products and are presented in Fig. 3. *W40* did not show any exothermic peaks, indicating that crystal growth has not occurred. The thermographs of *W50* and *W60* products contain one and two exothermic peaks, respectively. To define whether these peaks correspond to crystal growth and whether *W40* remains vitreous after annealing, a series of thermal treatments were conducted at temperatures given in Table 2. Annealing temperature for *W40* was chosen in order to be close to the endothermic peak located at 965 °C. In the case of *W50* and *W60* products, annealing temperatures were in the region of the exotherms and at a temperature above the exothermic peaks.

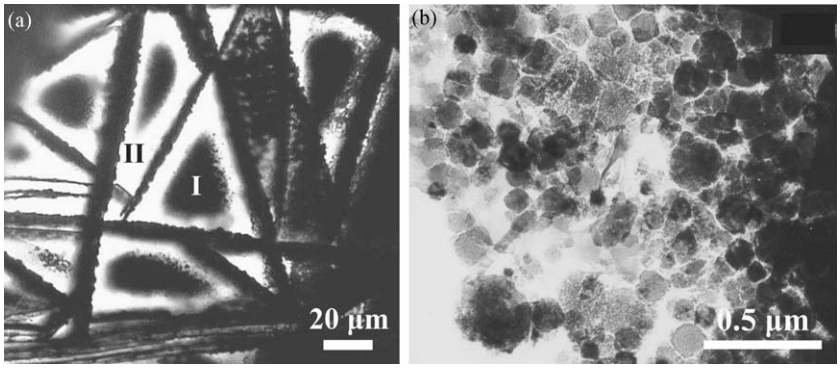

Fig. 2. (a) Optical micrograph of a thin slice of *W70* product observed under transmitted illumination. Regions denoted by I and II correspond to opaque (polycrystalline) and transparent (glassy) areas, respectively. (b) BF TEM micrograph of a thinned opaque area consisting of hematite and magnetite microcrystals.

Table 2
Effect of the thermal treatments on the microstructure of the vitrified products

Devitrified product	Annealing temperature (°C)	Dominant separated crystal phases	Structure
DW40	950	–	Vitreous
DW50a	700	$Pb_8Fe_2O_{11}$ (nuclei)	Primarily vitreous
DW50b	900	$Pb_8Fe_2O_{11}$	Glass-ceramic
DW60a	560	$PbFe_{12}O_{19}$	Glass-ceramic
DW60b	720	$PbFe_{12}O_{19} + Fe_2O_3$	Glass-ceramic
DW60c	900	Fe_2O_3	Glass-ceramic

3.3. Products of the devitrification process

The *W40* glass was not devitrified, when it was subjected to the annealing conditions shown in Table 2 (*DW40* product). The matrix remained amorphous, virtually intact from the thermal processes, to the resolution limit of TEM and HRTEM. However, comparison of the microprobe EDS analyses listed in Table 3, before and after annealing designated an effect of this process. With the exception of Si, the elemental composition presented a broader range of deviation values after thermal treatment. This indicates that the vitreous matrix has become less homogeneous, possibly due to alkali microsegregation.[15]

Conversely, thermal treatment of the *W50* glass resulted in crystal phase separation. After annealing at 700 °C, spherical nanocrystallites were nucleated, which were dispersed in the whole volume of the matrix (*DW50a* product). Fig. 4 is a HRTEM micrograph illustrating the crystal nuclei inside the vitreous matrix. The inset shows a magnified view of the micrograph depicting a crystal nucleus with well-defined lattice fringes. The spherical nanocrystallites were composed of Pb, Fe and O, as it was detected by microprobe analysis. However, when analyzing small size crystals embedded in a matrix, the electron beam intersects a cylinder that contains also the matrix and due to the larger excited volume, X-rays from a broader region are obtained. Thus, the relative proportion of the constituent elements could not be accurately specified. In order to obtain sizeable crystallites, as-quenched samples were annealed at 800 °C and cooled down throughout several hours (*DW50b* product). This method is usually referred to as the petrurgic method and gave rise to extensive growth of the dominant separated crystal phase, with crystallite sizes of the order of a few micrometers. Fig. 5 is an optical micrograph with some of the crystallites that separated from the parent glass matrix. The micrograph was obtained from a thin slice of *DW50b* product under transmitted illumination.

Table 3
Standard deviations of the elemental composition (at.%) of the *W40* matrix before and after thermal treatment, obtained by microprobe analysis

Element	As-quenched	950 °C
Fe	17.0	24.5
Pb	16.5	24.0
Si	10.5	8.6
Na	47.0	72.0

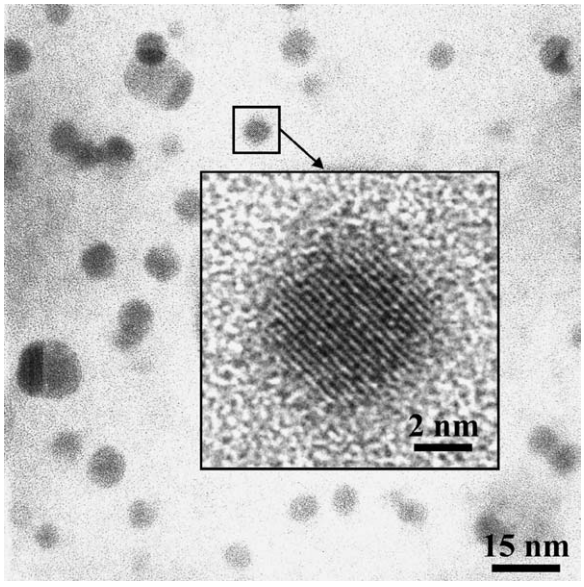

Fig. 4. HRTEM micrograph showing the nucleation of spherical nanocrystallites homogeneously dispersed in the matrix of the *DW50a* product. The inset is a magnified view of the nanocrystallite delimited in the square, depicting well-defined crystal lattice fringes.

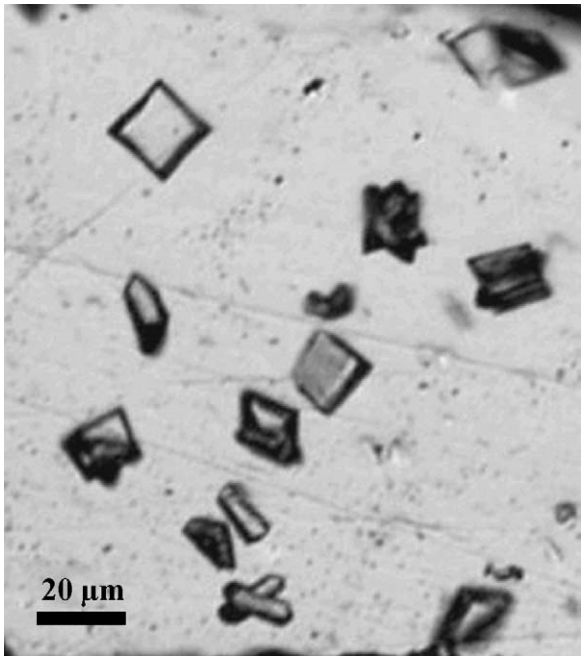

Fig. 5. The petrurgic method resulted to the growth of sizeable crystallites that were used to perform tilt-rotation TEM experiments.

Numerous EDS analyses, performed on these sizeable crystallites, have shown that the Pb/Fe atomic ratio is close to 4. X-ray powder diffraction files (PDF) do not contain a mixed lead–iron oxide with such an atomic ratio. In addition, selected area diffraction patterns (SADs) could not be attributed to any known structure of these elements. In order to characterize this separated crystal phase, a number of high symmetry SADs were obtained from various single crystallites. Wide-angle tilt-rotation TEM experiments were carried out to determine the characteristic extinction rules of the different reflections. The experimental procedure comprises the detection of at least one high symmetry zone axis (axis with low indices reflections) of the new crystal phase, followed by successive tilting about a low indices reflection belonging to the initial zone, and rotating, repeatedly about another low indices reflection when a new high symmetry zone axis is placed parallel to the electron beam. Such a successive tilting allows the user to find and exclude from the analysis the double diffracted reflections. In Fig. 6, a BF image of a single crystallite of the new phase oriented along a [0 0 1] zone axis of the tetragonal system is shown. Diffraction patterns 1–5 (primary zone axis is the [0 0 1]) and 6–7 (primary zone axis is the [0 1 0]) were obtained sequentially by tilting the crystallite about the axes designated in each one of them. The encircled diffraction spots denote the common reflections with the preceding diffraction pattern.

Eventually, this phase was characterized to be a lead–iron oxide of tetragonal symmetry with a molecular formula $Pb_8Fe_2O_{11}$, and lattice parameters $a = 0.580$ nm and $c = 1.437$ nm. The accuracy of these measurements is of the order of ± 0.005 nm. Computer simulation of the zone axes, based on these lattice parameters, verified the indexing of the experimental SADs presented in Fig. 6. The values of the a and c lattice parameters are directly calculated from 1 0 0 and 0 0 1 reflections of the [0 0 1] and [0 1 0] zone axes, respectively.

Devitrification of the *W60* glass, subsequent to annealing at 560 °C, has stimulated nucleation and growth of magnetoplumbite, which is a lead–iron oxide with a molecular formula $PbFe_{12}O_{19}$ (*DW60a* product). Magnetoplumbite crystallizes in the hexagonal crystal system ($a = 0.587$ nm, $c = 2.301$ nm) in the form of hexagonal flakes. Fig. 7(a) is a HRTEM micrograph, where the basal plane of the emerged crystal phase is shown. The perfect crystal structure of the flake, at atomic level, is illustrated in Fig. 7(c), which is a magnified part of Fig. 7(a). Three equally spaced families of lattice fringes at an angle of 120° to each other are denoted in Fig. 7(c). The common interatomic distance was found

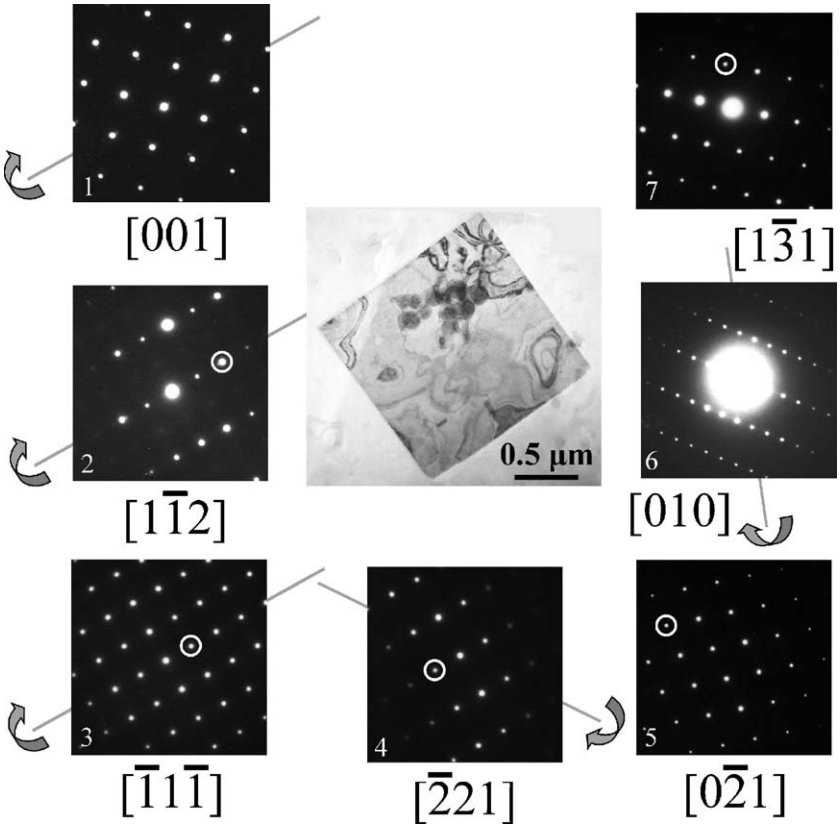

Fig. 6. Identification of the new mixed Pb–Fe oxide in the *DW50b* product by tilt-rotation TEM experiments. The sense of tilting about an axis parallel to a specific reflection in each SAD, in order to acquire the subsequent crystal zone axis, is denoted. The encircled diffraction spots denote the common reflections with the preceding SAD. Analysis of the SADs showed the presence of tetragonal $Pb_8Fe_2O_{11}$ crystallites inside the vitreous matrix. The central BF image depicts one of these crystallites with the [0 0 1] zone axis parallel to the electron beam.

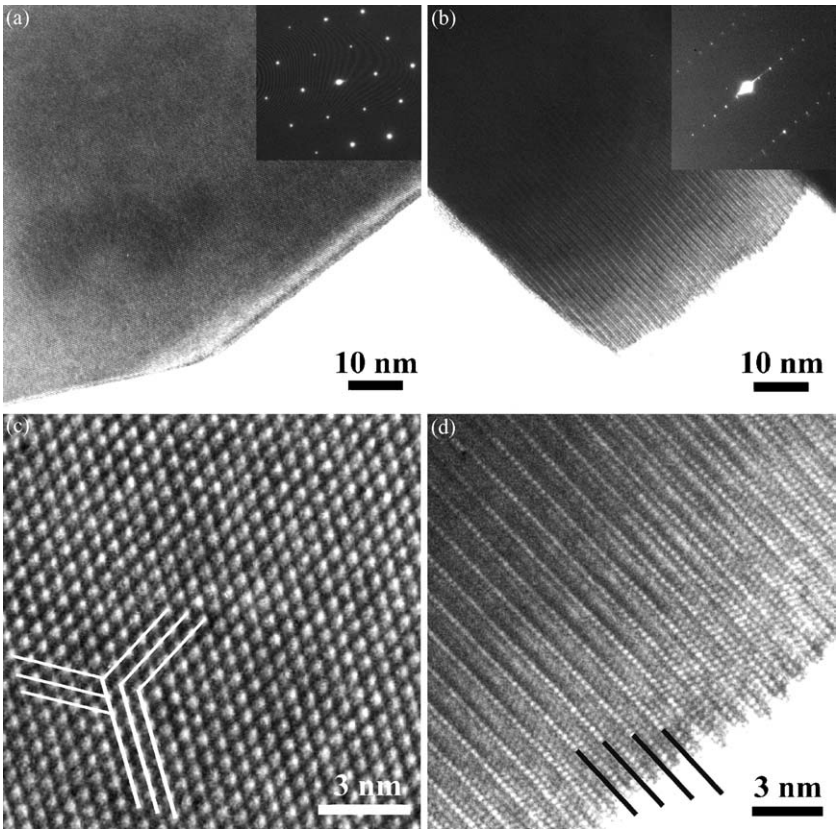

Fig. 7. HRTEM micrographs of a magnetoplumbite hexagonal flake, viewed (a) along and (b) normal to the *c* axis are shown. The corresponding diffraction patterns are given as insets. Micrographs (c) and (d) illustrate magnified areas of (a) and (b), respectively, revealing the crystal structure of magnetoplumbite in the atomic level.

to be 0.509 nm that matches the interplanar spacing of the $\{10\bar{1}0\}$ planes of magnetoplumbite (0.5086 nm). Fig. 7(b) is a HRTEM micrograph of a magnetoplumbite crystallite viewed along the $\langle 10\bar{1}0\rangle$ axis. Moreover, Fig. 7(d) is a magnified area of Fig. 7(b), where the lattice periodicity along the (0 0 0 1) axis is clearly observed. The black lines have been drawn with an interval of 1.15 nm, corresponding to the *c*/2 periodicity of magnetoplumbite. Therefore, the contrast difference, which is observed every three atomic layers can be attributed to the periodic variation of composition that arises due to the presence of Pb atoms within the atomic layers.

Annealing of the *W60* glass at higher temperature (720 °C) resulted in surface nucleation and growth of hematite alongside magnetoplumbite (*DW60b* product). Hematite crystallizes in the rhombohedral crystal system (*P3* space group), having lattice parameters $a = 0.556$ nm and $c = 2.255$ nm in the hexagonal description of the crystal lattice. In this case, extended foils of hematite grew from the surface of the samples towards the interior. The growth of hematite reaches a depth of $\cong 1\,\mu$m generating a magnetoplumbite-depleted zone.[11] This was established by thermally treating coarse-grained powder of *W60* glass at 900 °C (*DW60c* product). In this case, only hematite crystallites were present in the volume of the annealed product, due to the significant active surface area of the original material. Fig. 8 shows consecutive parallel layers of extended hexagonal foils, which have grown from the surface of the *DW60c* sample. The two inserted diffraction patterns (a) and (b) were obtained with the electron beam parallel to the $[1\bar{2}1\bar{3}]$ and $[\bar{2}4\bar{2}3]$ zone axes, respectively.

The effects of the annealing processes on the microstructure of the vitrified products are summarized in Table 2.

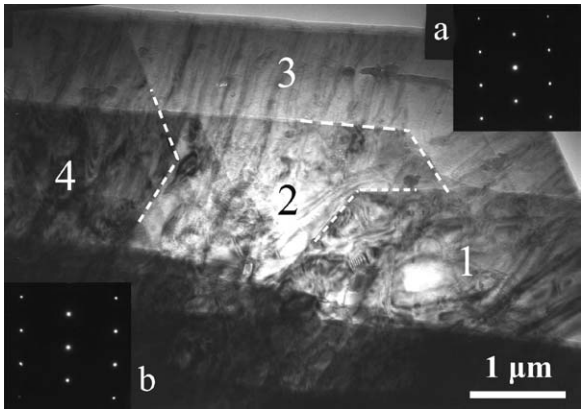

Fig. 8. Crystal growth of hematite from the surface of the devitrified *DW60c* product in the form of extended foils. The inset diffraction patterns, corresponding to (a) $[1\bar{2}1\bar{3}]$ and (b) $[\bar{2}4\bar{2}3]$ zone axes, were obtained from crystallite 3.

4. Discussion

All as-casted and thermally treated products that have been investigated in this work, except *DW60b* and *DW60c*, were chemically stabilized; i.e. the toxic agent (lead) cannot be leached away when the samples suffer the corrosive influence of acetic acid (TCLP protocol).[11] In the case of as-quenched vitreous products, the lead content is dispersed in the amorphous matrix. This conclusion is based on the results of EDS elemental analyses. Lead oxide, for the batch compositions listed in Table 1, is a glass network modifier,[16–18] and therefore, is bonded to the SiO_4 tetrahedra by electrostatic bonding.[19]

Iron oxide, in the form of ferrous oxide (FeO), is also a glass network modifier;[20] additionally, it can also act as a crystallization precursor.[21] On the other hand, iron oxide in the Fe^{3+} state (ferric oxide) is an intermediate and can function either as a glass network former or as a modifier, depending upon the glass composition.[19] The evidence that ferric oxide acted as a glass former, in our case, is derived from the fact that *W50* and *W60* products were vitreous. This observation seems to be at variance with the theory of oxide glass formation, according to which a Si/O ratio below 0.33 corresponds to a structure of broken (depolymerized) $[SiO_4]^{2-}$ chains. This kind of structure belongs to the class of "invert glasses".[4,22] Moreover, in the case of Si/O = 0.25 (*W60* product) the "glass" structure is constituted of isolated $[SiO_4]^{4-}$ units, i.e. one silicon atom is bonded with four non-bridging oxygen atoms. Therefore, under normal circumstances, these materials are expected to present low viscosity and a high tendency to crystallize instead of forming a vitreous network upon cooling. Thus, it is plausible to assume that ferric oxide functioned as a glass network former, sustaining the integrity of the glass network in the *W50* and *W60* vitrified products.

W70 multiphase product showed a different morphology compared to the as-quenched products that contained lower concentration of waste. This can be attributed to: (a) the high concentration of waste and (b) the rapid crystal phase separation during quenching and not throughout thermal treatment. In this case, crystal growth activated a diffusion process, which resulted in absorption of iron and oxygen mainly from neighbouring vitreous matrix regions.

The devitrification process gave rise to crystal phase separation in the *W50* and *W60* glasses, while *W40* was not receptive to detectable devitrification, under the annealing conditions applied to all vitreous samples. The structural stability of *W40* glass should rely on the fact that devitrification in such multi-component systems is based on reconstructive transformations.[19] Since the separated crystal phases have a different composition from the matrix, crystal growth demands rupture of bonds and long-range diffusion. It seems that the above two conditions are not fulfilled in the case of *W40*, due to its high SiO_2 content. As a result, it possesses a vitreous matrix with the highest structural integrity and the highest viscosity in the annealing temperatures relative to the *W50* and *W60* vitrified products.

Annealing of the *W50* and *W60* glasses resulted in the formation of new crystal phases. The firstly reported $Pb_8Fe_2O_{11}$ and $PbFe_{12}O_{19}$ (magnetoplumbite), which were the dominant phases grown in the matrices of the *W50* and *W60* glasses, respectively. In these crystal phases, iron takes part in the form of ferric oxide, since their chemical formula can be written as $(PbO)_8{\cdot}Fe_2O_3$ and $PbO{\cdot}(Fe_2O_3)_6$. EM observations from different cut sections of the devitrified samples suggested that the mechanism of nucleation is bulk nucleation. Moreover, hematite was formed on the surface of the *W60* glass at higher temperatures in relation to $PbFe_{12}O_{19}$. The growth of hematite can be attributed to the surface oxidation of Fe^{2+} to Fe^{3+}.[12,23,24] In this case both magnetoplumbite and hematite crystal phases coexisted.

Bulk nucleation of the two lead–iron oxides does not have an impact on the chemical stability.[10] In contrast, surface nucleation and growth of hematite impairs the chemical stability and the lead concentration in the leachate is comparable to that of the incinerated residue.[11] Hematite grows in the form of extended foils creating a dense network of crystallites on a surface layer of $\cong$1 μm thick. Furthermore, growth of hematite suppresses the crystal separation of magnetoplumbite through the formation of the surface layer, where the latter phase is depleted. This was confirmed by annealing a coarse-grained *W60* glass; in this case only hematite crystallites were detected, since the active surface area of the original material is substantial.

Accordingly, bulk crystallization involves crystal phase separation from the matrix of oxides that function as glass network formers and modifiers. This seems to produce a vitreous network that, as in the vitrified products, is capable of stabilizing lead atoms, while lead that participates in the formation of crystallites cannot be leached away from $Pb_8Fe_2O_{11}$ and $PbFe_{12}O_{19}$ crystal phases. Conversely, when hematite crystallizes, the vitreous matrix is depleted from a significant content of one of its formers (ferric oxide), while the lead content remains in the residual matrix. Consequently, the vitreous matrix loses its initial structural integrity, since an extended silica-based glass network cannot be formed and thus, lead can be leached away easily.

5. Conclusions

The evolution of microstructure of the as-quenched products during thermal treatment depends on waste content. Among the thermally treated materials, the *W40* glass was not receptive to devitrification. Conversely, in the annealed *W50* and *W60* glasses lead was separated from the vitreous matrix by volume crystallization forming $Pb_8Fe_2O_{11}$ and $PbFe_{12}O_{19}$ (magnetoplumbite) crystallites, respectively. $Pb_8Fe_2O_{11}$ is a newly reported tetragonal mixed lead–iron oxide acting as a "sink" of the toxic element. At high temperature annealing of the *W60* glass the Pb content remains in the residual matrix and surface crystallization of Fe_2O_3 occurs. Higher waste concentration than 60 wt.% results in the production

of a multiphase material, where hematite and magnetite separate from the glass matrix. The iron content of the waste in the form of ferric oxide participates in the construction of the glass network and, therefore, enhances its structural integrity. Thus, stable vitreous products can be formed with Si/O ratios as low as 0.25. Lead, on the other hand, is stabilized in the volume of the glass matrix or takes part in the growth of mixed lead–iron oxides.

Acknowledgement

The authors wish to thank the Greek Ministry of Education and Religious Affairs and European Union for financial support through the EPEAEK II "Pythagoras" program.

References

1. Colombo, P., Brusatin, G., Bernardo, E. and Scarinci, G., Inertizxation and reuse of waste maerials by vitrification and fabrication of glass-based products. *Curr. Opin. Sol. Stat. Mater. Sci.*, 2003, **7**, 225–239.
2. Romero, M., Rawlings, R. D. and Rincón, J. M., Development of a new glass-ceramic by means of controlled vitrification and crystallization of inorganic wastes from urban incineration. *J. Eur. Ceram. Soc.*, 1999, **19**, 2049–2058.
3. Haugsten, E. and Gustavson, B., Environmental properties of vitrified fly ash from hazardous and municipal waste incineration. *Waste Manag.*, 2000, **20**, 167–176.
4. Pisciella, P., Crisucci, S., Karamanov, A. and Pelino, M., Chemical durability of glasses obtained by vitrification of industrial wastes. *Waste Manag.*, 2001, **21**, 1–9.
5. Pelino, M., Recycling of zinc-hydrometalurgy wastes in glass and glass-ceramic materials. *Waste Manag.*, 2000, **20**, 561–568.
6. Barbieri, L., Corradi, A. and Lancellotti, I., Alkaline and alkaline-earth silicate glasses and glass-ceramics from municipal and industrial wastes. *J. Eur. Ceram. Soc.*, 2000, **20**, 2477–2483.
7. Scarinci, G., Brusatin, G., Barbieri, L., Corradi, A., Lancellotti, I., Colombo, P. *et al.*, Vitrification of industrial and natural wastes with production of glass fibers. *J. Eur. Ceram. Soc.*, 2000, **20**, 2485–2490.
8. Sheng, J., Vitrification of borate waste from nuclear power plant using coal fly ash. (II) Leaching behavior of the FA30 glass. *Fuel*, 2002, **81**, 253–256.
9. Tzeng, C. C., Kuo, Y. Y., Huang, T. F., Lin, D. L. and Yu, Y. J., Treatment of radioactive wastes by plasma incineration and vitrification for final disposal. *J. Hazard. Mater.*, 1998, **58**, 207–220.
10. Dwivedi, A., Berta, Y. and Speyer, R. F., Effect of controlled crystallization on the chemical durability of a lead-containing waste glass. *J. Mater. Sci.*, 1994, **29**, 2304–2308.
11. Kavouras, P., Kaimakamis, G., Ioannidis, T. A., Kehagias, Th., Komninou, P., Kokkou, S. *et al.*, Vitrification of lead-rich solid ashes from incineration of hazardous industrial wastes. *Waste Manag.*, 2003, **23**, 361–371.
12. Kavouras, P., Komninou, P., Chrissafis, K., Kaimakamis, G., Kokkou, S., Paraskevopoulos, K. *et al.*, Microstructural changes of processed vitrified solid waste products. *J. Eur. Ceram. Soc.*, 2003, **23**, 1305–1311.
13. Kavouras, P., Komninou, P. and Karakostas, T., Effect of composition and annealing temperature on the mechanical properties of a vitrified waste. *J. Eur. Ceram. Soc.*, 2004, **24**, 2095–2102.
14. Doremus, R. H., *Glass Science and Technology*. John Wiley and Sons, 1994.
15. Clark, D. E., Hench, L. L. and Acree, W. A., Electron microprobe analysis of Na_2O–CaO–SiO_2 glass. *J. Am. Ceram. Soc.*, 1975, **58**, 531–532.
16. Wang, P. W. and Zhang, L., Structural role of lead in lead silicate glasses derived from XPS saectra. *J. Non-Cryst. Sol.*, 1996, **194**, 129–134.
17. Fayon, F., Landron, C., Sakurai, K., Bessada, C. and Massiot, D., Pb^{2+} environment in lead silicate glasses probed by Pb–L_{III} edge XAFS and ^{207}Pb NMR. *J. Non-Cryst. Sol.*, 1999, **243**, 39–44.
18. Fayon, F., Bessada, C., Massiot, D., Farnan, I. and Coutures, J. P., ^{29}Si and ^{207}Pb NMR study of local order in lead silicate glasses. *J. Non-Cryst. Sol.*, 1998, **232–234**, 403–408.
19. Zarzycki, J., *Glasses and the Vitreous State*. Cambridge University Press, 1991.
20. Holland, D., Mekki, A., Gee, I. A., McConville, C. F., Johnson, J. A., Johnson, C. E. *et al.*, The structure of iron silicate glass—a multi-technique approach. *J. Non-Cryst. Sol.*, 1999, **253**, 192–202.
21. Karamanov, A. and Pelino, M., Crystallization phenomena in iron-rich glasses. *J. Non-Cryst. Sol.*, 2001, **281**, 139–151.
22. Shelby, J. E., *Introduction to Glass Science and Technology*. RSC Paperbacks, 1997.
23. Karamanov, A., Pisciella, P. and Pelino, M., The crystallization kinetics of iron rich glass in different atmospheres. *J. Eur. Ceram. Soc.*, 2000, **20**, 2233–2237.
24. Karamanov, A., Taglieri, G. and Pelino, M., Iron-rich sintered glass-ceramics from industrial wastes. *J. Am. Ceram. Soc.*, 1999, **82**, 3012–3016.